TITLE:

Closed Loop Control between Two GTPase Switches makes the Secretory Functions of the Golgi Responsive to Growth Factors

Lingxia Qiao[1†], I-Chung Lo[2†], Krishna K. Midde[2], Nicolas Aznar[2], Amer Ali Abd El-Hafeez[2¶], Inmaculada Lopez-Sanchez[2], Vijay Gupta[2], Marilyn G. Farquhar[2], Padmini Rangamani[1*] and Pradipta Ghosh[2, 3, 6, 8*]

Affiliations:

[1]Department of Mechanical and Aerospace Engineering, Jacob's School of Engineering, University of California San Diego, La Jolla, CA.
[2]Department of Cellular and Molecular Medicine, School of Medicine, University of California San Diego, La Jolla, CA.
[3]Department of Medicine, School of Medicine, University of California San Diego, La Jolla, CA.
[4]Department of Pediatrics, School of Medicine, University of California San Diego, La Jolla, CA.
[5]Department of Computer Science and Engineering, Jacob's School of Engineering, University of California San Diego, La Jolla, CA.
[6]Rebecca and John Moore Comprehensive Cancer Center, University of California San Diego.
[7]Skaggs School of Pharmacy and Pharmaceutical Science, University of California San Diego, La Jolla, CA.
[8]Veterans Affairs Medical Center, La Jolla, CA.

[†]These authors contributed equally.

***Correspondence to:**

Padmini Rangamani, Ph.D.; Professor, Department of Mechanical and Aerospace Engineering, University of California San Diego; 9500 Gilman Drive (MC0411), La Jolla, CA 92093.
Phone: 858-534-4734. Email: prangamani@ucsd.edu

Pradipta Ghosh, M.D.; Professor, Departments of Medicine and Cellular and Molecular Medicine, University of California San Diego; 9500 Gilman Drive (MC 0651), George E. Palade Bldg, Rm 232, 239; La Jolla, CA 92093. Phone: 858-822-7633. Email: prghosh@ucsd.edu

¶ **Secondary Affiliation**: Pharmacology and Experimental Oncology Unit, Cancer Biology Department, National Cancer Institute, Cairo University, Cairo, Egypt

Abbreviations: GIV, Gα-interacting Vesicle-associated protein; GEM, guanine nucleotide exchange modulator; DoRA, dose-response alignment; Arf1, ADP-ribosylation factor-1; EGF, Epidermal growth factor; ER, endoplasmic reticulum; ERGIC, ER-Golgi Intermediate Compartment; CLC, closed loop control; GGA, Golgi-localized, γ-ear-containing, Arf -binding protein.

GRAPHIC ABSTRACT

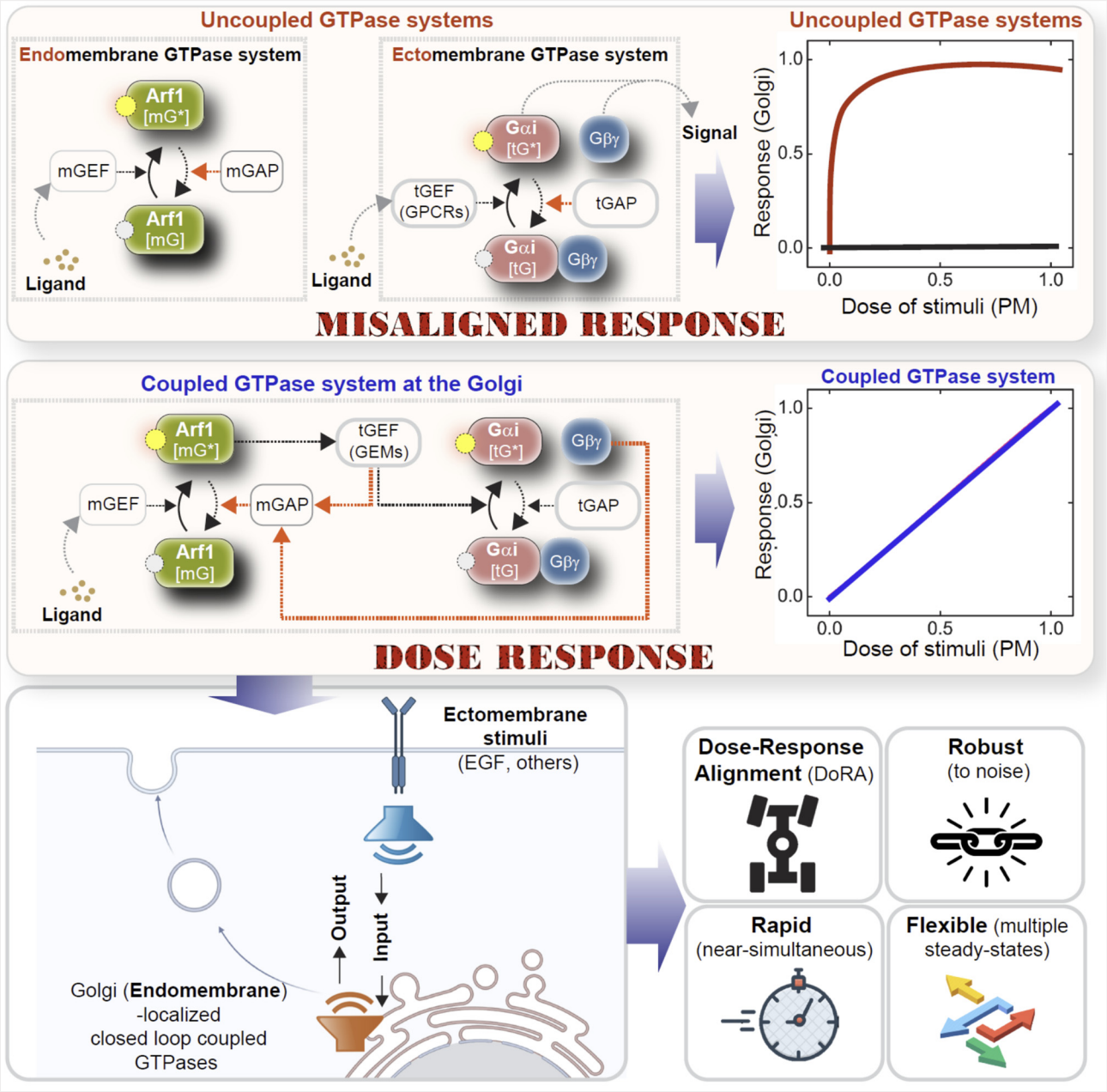

HIGHLIGHTS

- Endo- (mono) and ectomembrane (trimeric) GTPase systems are believed to function independently.
- Their coupling in a closed loop system at the Golgi makes cell secretion proportionate to stimuli.
- Coupling enables closed-loop mutual control of both GTPases and dose response alignment (DoRA).
- Uncoupling creates an open loop which generates misaligned and discordant responses.

SUMMARY:

Intercellular (between-cells) signals must be converted into an intracellular (within-cell) signal before it can trigger a proportionate response. How cells mount such proportionate responses within their interior remains unknown. Here we unravel the role of a coupled GTPase circuit on the Golgi membranes which enables the intracellular secretory machinery to respond proportionately to the growth factors in the extracellular space. The circuit, comprised of two species of biological switches, the Ras-superfamily monomeric GTPase Arf1, and the heterotrimeric GTPase, Gi$\alpha\beta\gamma$ and their corresponding GAPs and GEFs, is coupled *via* at least one a forward and two key negative feedback loops. Interrogation of the circuit featuring such closed-loop control (CLC) using an integrated systems-based and experimental approach showed that CLC allows the two GTPases to mutually control each other and convert the expected switch-like behavior of Arf1 into an unexpected dose response aligned (DoRA) linear behavior. Such behavior translates into growth factor stimulated Gi$\alpha\beta\gamma$ activity on Golgi membranes, temporal finiteness of Arf1 activity, and cellular secretion that is proportional to the stimuli. Findings reveal the importance of the coupled GTPase circuit in rendering concordant cellular responses *via* the faithful transmission of growth signals to the secretory machinery.

INTRODUCTION

To interact with their environment, mammalian cells produce ~ 2641 soluble proteins (signaling proteins, enzymes, hormones, antibodies, extracellular matrix proteins and structural components) and >5500 membrane proteins (*1*). For preparing and exporting those proteins to the extracellular environment, eukaryotic cells use an essential, efficient, and accurate molecular machinery, i.e., the protein secretory pathway. This pathway consists of various modules which are compartmentalized on the endoplasmic reticulum (ER) and the Golgi apparatus and are responsible for folding, processing of the post-translational modifications (PTMs), and trafficking of the proteins routed to the membrane of extracellular space (*2, 3*).

Originally believed to be a constitutive function that is regulated by 'housekeeping' genes/proteins that maintain the integrity of the local (membrane or lumenal) environment (*4*), the secretory pathway is now believed to be highly responsive to the extracellular signals. For example, an unbiased analysis of the genes that regulate the secretory pathway in diverse tissues indicated that the pathway is responsive to tissue-specific context and extracellular cues (*5*). Similarly, inhibitors of growth factor signaling (e.g., EGFR inhibitors) impact Golgi structure and secretion in a dose dependent manner as does the Arf1 inhibitor and fungal metabolite, Brefeldin A (BFA) (*6*). Furthermore, others have shown that tyrosine phosphorylation and dephosphorylation cascades may be important for budding of vesicles from the ER, ERGIC and the Golgi (*7*). But the first and the only concrete evidence that secretion is regulated by exogenous growth factors emerged in 2008 when the phosphoinositide phosphatase SAC1 was implicated as a 'brake' in anterograde Golgi secretion that is released by growth factors (*8*). By contrast, in the case of retrograde Golgi to ER transport, conflicting reports exist; while some (*9*) posit that either EGF or PDGF can trigger retrograde transport while others disagree (*10*). Thus, although the molecular biology and biochemistry of the secretory pathway are well-studied for its core components (*11-13*), what remains unknown to date is if and how the secretory system (or any intracellular organelle/system) responds proportionately to the external cues.

RESULTS AND DISCUSSION

Modeling a closed loop system of two Golgi-localized GTPases, monomeric Arf1 and trimeric Giα•βγ

Here we use a transdisciplinary approach to dissect the role of an endomembrane GTPase circuit at the Golgi (**Figure 1A-B**) which dynamically couples two unlikely and distinct species of biological switches that gate signal transduction (**Figure S1**; *top*), i.e., small or monomeric (m) and heterotrimeric (t) GTPases. The first evidence for the existence of this circuit emerged in 2015 (*14*). Before that, mGTPases are mostly believed to function within the cell's interior and are primarily concerned with organelle function and cytoskeletal remodeling (*15-17*). tGTPases, on the other hand, were believed to primarily function at the plasma membrane (PM) from where they gate the duration, type and extent of signals that are initiated by receptors on the cell's surface (*18*). Using a combination of biochemical, biophysical, structural modeling, live cell imaging, and numerous readouts of Golgi functions, it was shown that the mGTPase-Arf1 and the tGTPase Gi co-regulate each other on the Golgi through one key forward reaction (Arrow 1, **Figure 1B**; recruitment of GIV/Girdin, the GEF for tGTPase Gi by active Arf1) and a set of two feedback loops that culminate in the maximized activation of ArfGAP2/3, which terminates Arf1 signaling (Arrows 2 and 3, **Figure 1B**, **Figure S1**; *bottom*) (*14*). This phenomenon of co-regulation between the two classes of GTPases was shown to be critical for maintaining Golgi shape and function at steady states. The triggers for or the consequence(s) of such co-regulation on signal sensing/response remained unknown.

Because coupling of two species of GTPase switches, Arf1 and Gi, with feedback control is likely to generate complex, nonlinear, and non-intuitive emergent properties and, in turn, regulate secretion at the Golgi, we developed a computational model for this coupled circuit, using the general framework presented in (*19, 20*) (see **Supplementary Online Materials**). We asked if and how coupling and mutual coregulation impacted the temporal finiteness of either GTPase signaling and/or the alignment of secretory responses to the input signal, i.e., growth factors. For the purposes of modeling, we assumed the finiteness of Arf1 activation-inactivation cycle a surrogate indicator of successful anterograde cargo movement through the major compartments (i.e., ERGIC to the Golgi) within the secretory pathway because Arf1 regulates membrane traffic through a cycle of GTP binding and hydrolysis (*21*)-- GTP binding is a pre-requisite for membrane curvature and vesicle formation (*22*) from the donor compartment, whereas GTP hydrolysis is a pre-requisite for vesicle uncoating (*23*) and fusion with acceptor compartment. The steps that involve membrane mechanics when converting the Arf1 activity to secretion, were also modeled using Hill-type kinetics to capture the switch-like behavior. All governing equations were modeled using Hill-type equations based on logic operators such that the activity of each species varies between 0 and 1 (*24, 25*).

EGF activates Arf1 (mG*) at the Golgi and triggers the recruitment of a GEF for trimeric Giα•βγ

We first asked if this circuit of coupled GTPases responds to external stimuli. The stimuli we prioritized in this study is growth factors, and more specifically epidermal growth factor (EGF) because of prior evidence documenting its role in the regulation of Golgi secretion (*8*), its fragmentation during mitosis (*26*), and most

importantly, in the activation of Arf1 (*27-29*). We began by measuring the very first event in the circuit, i.e., the modulation of Arf1 activity by EGF using a previously validated pull-down assay that uses the GST-GAT domain of GGA3 to selectively bind the active GTP-bound pool of Arf1(*30*) (**Figure 1C**). The levels of Arf1•GTP were increased ~3-fold within 5 min after ligand stimulation, followed by a return to near baseline by 30 min (**Figure 1D-E**). These temporal dynamics of Arf1 activation-inactivation after EGF stimulation was used to fit the parameters for Arf1 activity in the computational model of the circuit (**Figure 1F**) (R2 and normalized RMSE are 0.72 and 0.19 respectively; see **Supplementary Online Materials** for model parameters). Such fitting completed the characterization of the first GTPase switch, i.e., Arf1; in this case, the input is ligand stimuli (EGF) and the output is Arf1-GTP (OUTPUT #1; mG*).

The immediate and key consequence of Arf1 activity within the coupled GTPase circuit is the first segment of the feed-forward loop, i.e., the recruitment of an effector of mGTPase Arf1 and a guanine nucleotide exchange factor of tGTPase Gi, GIV/Girdin (*14*). An evolutionarily conserved region in the N-terminal Hook domain of GIV bearing semblance to the 'Hook-like patch' on GGA-GAT domain (*31-34*) was shown to directly and preferentially bind to the active GTP-bound conformation of Arf1 (*14*). Because active Arf1 regulates membrane association of GIV (*14*) and several proteins are involved in vesicle trafficking (*21*), we asked if ligand-dependent activation of Arf1 was also associated with the recruitment of GIV. By immunofluorescence microscopy we confirmed that membrane-colocalization of Arf1 and GIV was increased within 5 min after ligand stimulation compared to serum-starved control cells (**Figure 1G**). A quantification the Arf1-positive Golgi regions using a Mander's overlap coefficient (MOC) confirmed that the EGF-induced increase in the degree of colocalization between Arf1-HA and GIV fluorophores was significant (**Figure 1H**). These results indicate that EGF activates mG* at the Golgi, and the latter triggers the recruitment of a GEF for trimeric Giα•$\beta\gamma$ (**Figure 1I).**

EGF triggers the activation of Gi (tG*) on Golgi membranes

We next evaluated the second segment of the feed-forward loop, i.e., GIV's ability to bind and activate the tGTPase Gi on Golgi membranes (**Figure 2A**). GIV does so using its C-terminal GEM motif, the structural basis for which has now been resolved (*35*). To this end, we used a previously well-established FRET-based assay in living cells (*36*) in which the dissociation of Gαi_1-YFP and CFP-G$\beta_1\gamma_2$ (low FRET) is used as a surrogate marker for 'activation' of Gi (**Figure 2B**). Using these constructs in living cells, we previously showed that Gαi1-YFP localized to two major sites, i.e., the Golgi and the PM. While most of the Gαi at the PM stays complexed with G$\beta\gamma$ as inactive heterotrimers, a significant portion of the Golgi-localized pool is found to be dissociated (*14*). When serum-starved cells were stimulated with EGF, we found that in cells with GIV (control cells) there was a significant drop in FRET both at the Golgi and at the PM within 5 min after EGF stimulation (**Figure S2A-B**). The extent of drop in FRET in the Golgi region, indicative of trimer dissociation at the Golgi, continued to peak by 15 min, reaching a plateau by 25-30 min after EGF stimulation (**Figure 2D-E**; **Figure S2A-B**). The delay in the activation of tGTPase relative to the mGTPase is consistent with previous observations that propagation of signal

from the extracellular space to the cell interior takes longer than PM-proximal events (*37*). These experimentally observed dynamics of tGTPase activation at the Golgi (OUTPUT #2) in response to EGF (INPUT) in control cells matched model prediction with excellent fitness (R2 and normalized RMSE are 0.54 and 0.41 respectively; see **Supplementary Online Materials** for model parameters). Furthermore, our model predicted that EGF-induced tGTPase activation at the Golgi would be abolished in cells without GIV (shGIV), in which m- and tGTPases cannot be coupled within the circuit (**Figure 2D**). This prediction was experimentally validated in shGIV cells using the same FRET-based approach; the expected drop in FRET in the Golgi region was virtually abolished in these cells (**Figure 2C, 2E**). Using an anti-Gαi:GTP mAb, which specifically recognizes the GTP-bound active conformation of the Gαi (1/2/3) proteins (**Figure 2F**, *top*) (*38*), we further confirmed that EGF triggered-active Gαi was detected at the Golgi in control cells, where it colocalized with Man II (**Figure 2F**, *bottom*). Similar findings were seen also with 10% serum (representing a well-mixed growth factor stimuli) and lysophosphatidic acid (LPA), a ligand for the GPCR, LPAR (**Figure S2C-D**). Taken together, these results demonstrate that Gαi is activated at the Golgi upon EGF stimulation, and that such activation requires the coupling of the two GTPases by GIV.

EGF activates ArfGAP, terminates Arf1 signaling *via* feedback loops within the closed loop system

We next evaluated the feedback loops, which are critical for the 'closed loop' architecture of the circuit, i.e., deactivation of Arf1 (mG*) by ArfGAP2/3 (mGAP) (**Figure 2G**). Two negative feedback loops activate ArfGAP2/3 (arrows 2 and 3 in **Figure 2A**). Arrow 2 represents GIV's ability to bind and recruit ArfGAP2/3 to COPI vesicles and the Golgi membranes. Failure to recruit ArfGAP2/3 in GIV-depleted cells was implicated, in part, to the elevated levels of Arf1•GTP and stalled anterograde secretion in these cells (*14*). Arrow 3 represents the fact that GIV suppresses the levels of active Arf1 and regulates ERGIC→Golgi transport and Golgi structure in part *via* activation of Gi and release of 'free' Gβγ; GIV's GEF function (which activates Gαi) is required for this effect (*14*). We noted that by design, both negative feedback loops, arrows 2 and 3 depend on the forward reaction, arrow 1, which involves the recruitment of GIV (tGEF) (**Figure 1B**). Using the rate of deactivation of Arf1 after ligand stimulation as a readout, we next measured the activity of ArfGAP2/3 in control and GIV-depleted cells responding to EGF (**Figure 2H**). In parallel, we conducted simulations for the coupled circuit in the absence of either arrows 2 and 3, or when both are lost simultaneously in cells without GIV (**Figure 2I**). Such simulations transform the coupled GTPase switches from a closed loop with negative feedback to an open loop circuit sans such feedback (*39*). Simulations predicted that in shGIV cells, which lack both negative feedback loops, Arf1 activity after EGF stimulation will be sustained, disrupting the temporal finiteness of this signal (**Figure S3B**; red, **Figure 2I**). Simulations matched experiments closely -- Arf1 activity peaked within 5 min after EGF stimulation and rapidly reduced thereafter by 15 min in control cells but remained sustained until 15 min in GIV-depleted cells (**Figure 2H, S3A**). When we ran the simulations after disabling the two negative feedback arrows one at a time, the predicted dynamics of Arf1 activity (OUTPUT #1) in response to EGF (INPUT) mirrored that of having both loops disabled (as in shGIV cells) (**Figure 2I**). These findings suggest the existence of an 'AND gate'-like

digital logical operation (*40*), i.e., a HIGH output (ArfGAP2/3 activity, and resultant termination of Arf1 signaling) results only if both the inputs to the AND gate (arrows 2 and 3) are HIGH. If neither arrow or only one of the arrows (inputs to the AND gate) are HIGH, LOW output results. In signal transduction, such logical operations serve to integrate multiple input signals.

Finally, we sought to estimate the impact of the negative feedback loops on the activity of the tGTPase, Gi (OUTPUT #2) in response to EGF (INPUT). Model simulations predicted that the Gi activity was practically unaffected (maybe even slightly increased) when either negative feedback loop was removed (**Figure 2J**). Because experimental tools/approaches to specifically inhibit one negative feedback loop at a time do not exist at present, experimental validation of these predictions was not feasible. Regardless, these findings suggest that an AND gate of two negative feedback loops exerts the most dramatic effects on the mGTPase (Arf1) and has little or no effect on the activity of the tGTPase.

Coupling of two GTPases is required for EGF-triggered secretion of diverse cargo proteins

Because one of the major consequences of coupling two distinct species of GTPases, Arf1 and Gi via GIV at the Golgi are permissiveness to protein secretion (*14*), we next asked if the coupled circuit is required for growth factor-responsive secretion. To this end, we examined the transport of the transmembrane cargo protein, vesicular stomatitis virus G protein (VSVG), from the ER to the PM using the well-characterized GFP-tagged VSVG-tsO45 mutant (*41*). This mutant VSVG is retained in the ER at 40°C, accumulates in Golgi stacks at 20°C temperature block, from where it escapes to the PM at permissive 32°C (**Figure 3A**). Immunofluorescence studies were carried out in non-permeabilized cells using an anti-VSVG ectodomain antibody to selectively visualize the fraction of molecules that reached the cell surface; the intensity of GFP signals was used towards quantifying the total cellular pool of VSV-G protein. Considerable VSVG accumulated in the Golgi region in both control and GIV-depleted cells under serum starved conditions at 20°C. EGF or serum stimulation was permissive to transport of the VSV-G protein to the PM in control cells at 32°C, but such transport was significantly diminished in GIV-depleted cells (**Figure 3B-C**). Similar results were observed also in the case of EGF-stimulated secretion of three separate soluble cargo proteins, MMP2, MM9 (**Figure 3D-F**) and Collagen (**Figure 3G-H**); these cargo proteins were chosen because of GIV's published role in ECM degradation during cancer metastasis (*42*) and tissue fibrosis (*43*). Together, these findings show that when GIV-dependent coupling of Arf1•GTP with Gi is lost, the secretory functions of the Golgi are no longer responsive to growth factors.

Coupled GTPases enable high fidelity concordant Golgi response to EGF

Advantaged with an experimentally validated computational model of a naturally occurring circuit representing an unlikely coupling of two species of GTPases, we next asked how might coupling be beneficial to cells. More specifically, we asked how coupled (closed loop control) *vs*. uncoupled (open loop) systems impact mono- and

trimeric-GTPase signaling on endomembranes and organelle response, i.e., secretory functions of the Golgi in response to stimuli that is perceived at the ectomembrane. As shown in **Figures 1-3**, the temporal propagation of the input signal (EGF) takes ~5 min to trigger events at the Golgi. This is considerably delayed compared to most of the well-defined EGF-stimulated, receptor-proximal events (**Figure 4A**), i.e., receptor dimerization, autophosphorylation, and adaptor recruitment, all of which begin within ~2-5 sec of ligand stimulation, and plateau by 20-30 sec and begin to fade by 80-90 sec (*44*). Even the initiation of the downstream MAPK cascade begins by 10-20 sec after ligand stimulation (*44*). This delay is consistent with the concept of propagation delay in networks (*37*), defined as the amount of time it takes for the signal to travel from the sender (i.e., receptor at the PM) to the receiver at the interior of cells (i.e., Arf1 on the Golgi).

To gain insights into how coupling impacts responses to the input signal (EGF), we conducted simulations with the inclusion of noise within the EGF stimuli over a wide range of concentrations and compared the dose-response behavior at steady-states of the different outputs in coupled switches against a single switch (mG/G*). In the case of a single switch, both mGEF and mG* show classic dose-response curves (**Figure 4B**) but lack alignment. By contrast, in the coupled switches, mGEF and mG* both show the classic dose-response curves with increased alignment between mGEF and mG* at higher EGF doses (**Figure 4C**). The misalignment in the case of single switch is evident in plots of fractional activation of mG* for a given mGEF activity; a single Arf1 switch displays hyperresponsiveness, in that, max mG* is achieved even with minimal mGEF activity (**Figure 4D**). In the case of coupled switches, similar plots of fractional activation of mG* for a given mGEF activity show dose-response alignment with an unexpected linear relationship (**Figure 4E**). Although unexpected for a GTPase switch, this finding is consistent with what is generally expected in a closed loop with negative feedback control (*39*). The dose-response curves for tG* and secretion as a function of EGF both follow the expected ultrasensitive response in the case of coupled switches (blue lines; **Figure 4F, G**); both responses are misaligned in the case of single switch displaying hypo-responsiveness (red lines; **Figure 4F, G**). Because Arf1 activity-inactivity cycles are critical for cargo movement within the secretory pathway (*21*), and Arf1 activity shows a linear dose response to EGF (**Figure 4E**), our model predicts that the coupled switches with negative feedback can enable a proportionate response (output = secretion) to a given dose of stimuli (input = EGF) through intermediaries (mG* and tG*). The potency of such a response (secretion in coupled system) is almost as much as the potency of Arf1 activation by EGF in the single switch model (Hill coefficient as a single switch (EGF-mG*) n_{Hill}=1.79 for a single switch mG*/EGF, n_{Hill}=1.83 for the coupled switch secretion/EGF, **Figure 4H**).

To assess the degree of fidelity in the closed loop control system, we compared the input-output relationships for intermediaries in the circuit in the presence of intracellular noise [simulated within the concentrations of the different species (nodes) and the connections between them (arrows)] (see **Supplementary Online Materials** for details). For a single switch, the mGEF-mG* relationship displayed a Hill coefficient of 1.34 (**Figure 4I**), whereas the mGEF→mG* relationship (switch #1) in the coupled switches continued to display a linear response (**Figure 4J**) (*39*). The tGEF→tG* switch (switch #2) shows a dose-response behavior close to the saturation regime of an ultrasensitive curve (n_{Hill}=3.95) (**Figure 4K**) and the

tG*→secretion relationship shows a strong ultrasensitive response (n_{Hill}=12.04) (**Figure 4L**). Although the tG*→secretion step is currently represented within our model as a "black box", the strong ultrasensitive behavior of this step suggests that it could be controlled *via* other species of GTPases that are involved in membrane mechanics (e.g., curvature, fission, fusion, etc.). For example, the large GTPase dynamin, which is modulated by tG* (*via* 'free' Gβγ)-intermediates and is critical for vesicle scission from donor compartments. Similarly, SNARE proteins that are effectors of tG* (*via* 'free' Gβγ)-intermediates work cooperatively with Rab GTPases to ensure targeted vesicle fusion on acceptor compartments (*45*). Despite the ambiguity of what intermediaries constitute this step of membrane mechanics, information propagation via the closed loop coupled system appears to be robust to noise in the stimulus, noise in the concentrations of the species, and noise in the connections suggesting that the nature of the system afforded protection against variations in molecular activities at various stages of the pathway (*46*).

CONCLUSIONS

Much of the analysis of information propagation in signaling is focused on events at the PM and many emergent properties of such systems have been identified using systems biology but none thus far have coupled the events at the ectomembrane to the events at the endomembrane. The key outcome of this study is an experimentally validated model of a Golgi-localized natural coupling between the two GTPase switches with exquisite feedback control (**Figure 5A**) that enables linear activation of Arf1 in response to EGF, which in turn enables the Golgi to mount a response (protein secretion) that is proportionate to the stimuli and robust to noise. The model reveals three notable features of the nature of Golgi secretory response.

First, it is noteworthy that both PM-proximal events as well as the endomembrane-localized events peak simultaneously at ~5 min post EGF stimulation, e.g., EGF-triggered pERK (*47, 48*), coupling of ligand-activated EGFR to trimeric Gi at the PM (*49*), and Golgi localized events such as Arf1 activation (**Figure 4A**). Because cells frequently respond with high fidelity and specificity in an ultrasensitive fashion to graded input (*50*), such that a response is triggered only when signals reach peak levels and break thresholds, our findings imply that despite a propagation delay, there is virtually no latency between when these peak signals are reached. This implies that the cell's network is able to carry out near simultaneous conversations at the ecto(PM)- and the Golgi membranes, and the virtual lack of latency in peak signals indicates more responsiveness of the network so that the Golgi membranes can mount a rapid response to the events at the PM (**Figure 5C**).

Second, our findings show that the closed loop control system generated dose-response alignment (DoRA), enabling a linear increase in Arf1/mG* activation. Such DoRA has been described in several major receptor initiated signaling cascades at the PM (from the pheromone response system in yeast to the Wnt→βCatenin, TGFβ→SMAD2/3 and EGFR→MAPK cascades in mammals) (*51*), but never in endomembrane GTPases. Because a linear DoRA maximally preserves any information during its propagation, and many different cellular signaling systems avoid losing information by transmitting it in a linear manner (*52*), we conclude that one of the major discernible consequences of the closed loop coupling of two GTPases is its ability to faithfully transmit information from the PM to the Golgi for the latter to mount a concordant secretory response (**Figure 5C**).

Third, although the first switch, i.e., Arf1/mG* showed a linear response, each of the subsequent switches (switch #2 and the step of membrane mechanics leading to secretion) becomes progressively ultrasensitive. The net result of this is that the closed loop feedback control allows for a tighter alignment of secretion with respect to EGF by 'stretching' out the dose-response curve across series of switches to propagate the signal from the extracellular space to the interior of the cell (**Figure 5B**). Because the stability behavior of a mathematically simpler version of this closed loop system of coupled GTPases showed that coupling afforded a wide range of steady states (*53*), it is tempting to speculate that the coupled system allows flexibility in responses over a wide range of stimuli (**Figure 5C**).

In closing, despite tremendous advances in our understanding of cell-cell communication, lack of similar insights into intracellular signaling has prompted many to resort to oversimplified “black box” (*54*) models or model eukaryotic cells as a “well-mixed bag of molecules” (*55*). The model of Golgi-localized closed loop coupled GTPase circuit validated here begins to shed light upon how one organelle, i.e., the Golgi complex, carries out its key functions, i.e., protein secretion in a manner that is not only responsive to extracellular cues, but also how such response is rapid, proportionate to the stimuli and robust to noise.

ACKNOWLEDGEMENT

We thank Linda Joosen for technical assistance with FRET assays. This work was supported by the National Institute of Health Grants: CA238042, AI141630 and CA160911 (to P.G.), GM132106 (to P.R), CA100768 (to M.G.F and P.G). P.R was also supported by the Air Force Office of Scientific Research (AFOSR) Multidisciplinary University Research Initiative (MURI) Grant FA9550-18-1-0051. I-C. L. was supported in part by a Fellowship (NSC 100-2917-1-564-032) from the National Science Council of Taiwan, K.M. by Susan G. Komen award (# PDF14298952) and I.L-S by the American Heart Association (AHA #14POST20050025). A.A.A was supported, in part, by an NIH-funded Cancer Therapeutics Training Program (CT2, T32 CA121938).

AUTHOR CONTRIBUTIONS

L.Q carried out and analyzed all modeling studies in this work. I-C.L., C.R., A.A.A. designed, carried out and analyzed most of the experiments and assembled the figures. V.G. performed VSVG transport assays; N.A and I-C.L performed the MMP and collagen secretion assays. K.M. and I.L-S carried out and analyzed the FRET and Gαi:GTP assays, respectively. L.Q, AAA, I-C.L and V.G. helped write methods and edit the manuscript. P.G. and M.G.F conceptualized, designed, supervised and analyzed the experiments. P.R, with input from P.G, conceptualized, designed, supervised and analyzed the modeling studies. P.G and P.R wrote the manuscript.

DECLARATION OF INTERESTS

The authors declare no competing interests.

REFERENCES CITED

1. M. Uhlén *et al.*, Tissue-based map of the human proteome. *Science* **347**, (2015).
2. J. E. Rothman, L. Orci, Molecular dissection of the secretory pathway. *Nature* **355**, 409-415 (1992).
3. R. B. Kelly, Pathways of protein secretion in eukaryotes. *Science* **230**, 25-32 (1985).
4. P. Arvan, X. Zhao, J. Ramos‐Castaneda, A. Chang, Secretory pathway quality control operating in Golgi, plasmalemmal, and endosomal systems. *Traffic* **3**, 771-780 (2002).
5. A. Feizi, F. Gatto, M. Uhlen, J. Nielsen, Human protein secretory pathway genes are expressed in a tissue-specific pattern to match processing demands of the secretome. *NPJ systems biology and applications* **3**, 1-9 (2017).
6. G. Boncompain *et al.*, BML-265 and Tyrphostin AG1478 disperse the Golgi apparatus and abolish protein transport in human cells. *Frontiers in cell and developmental biology* **7**, 232 (2019).
7. C. D. Austin, D. Shields, Formation of nascent secretory vesicles from the trans-Golgi network of endocrine cells is inhibited by tyrosine kinase and phosphatase inhibitors. *The Journal of cell biology* **135**, 1471-1483 (1996).
8. A. Blagoveshchenskaya *et al.*, Integration of Golgi trafficking and growth factor signaling by the lipid phosphatase SAC1. *The Journal of cell biology* **180**, 803-812 (2008).
9. D. J. Gill, J. Chia, J. Senewiratne, F. Bard, Regulation of O-glycosylation through Golgi-to-ER relocation of initiation enzymes. *Journal of Cell Biology* **189**, 843-858 (2010).
10. G. G. Herbomel *et al.*, The GalNAc-T Activation Pathway (GALA) is not a general mechanism for regulating mucin-type O-glycosylation. *PloS one* **12**, e0179241 (2017).
11. P. Novick, S. Ferro, R. Schekman, Order of events in the yeast secretory pathway. *Cell* **25**, 461-469 (1981).
12. P. Novick, C. Field, R. Schekman, Identification of 23 complementation groups required for post-translational events in the yeast secretory pathway. *Cell* **21**, 205-215 (1980).
13. R. Schekman, L. Orci, Coat proteins and vesicle budding. *Science* **271**, 1526-1533 (1996).
14. I.-C. Lo *et al.*, Activation of Gαi at the Golgi by GIV/Girdin imposes finiteness in Arf1 signaling. *Developmental cell* **33**, 189-203 (2015).
15. E. E. Evers, R. A. van der Kammen, P. Jean, J. G. Collard, Rho-like GTPases in tumor cell invasion. *Methods in enzymology* **325**, 403-415 (2000).
16. S. Etienne-Manneville, A. Hall, Rho GTPases in cell biology. *Nature* **420**, 629-635 (2002).
17. Y. Takai, T. Sasaki, T. Matozaki, Small GTP-binding proteins. *Physiological reviews* **81**, 153-208 (2001).
18. A. G. Gilman, G proteins: transducers of receptor-generated signals. *Annual review of biochemistry* **56**, 615-649 (1987).
19. S. Cao *et al.*, Quantification of model and data uncertainty in a network analysis of cardiac myocyte mechanosignalling. *Philosophical Transactions of the Royal Society A* **378**, 20190336 (2020).
20. J. J. Saucerman, A. D. McCulloch, Mechanistic systems models of cell signaling networks: a case study of myocyte adrenergic regulation. *Progress in biophysics and molecular biology* **85**, 261-278 (2004).
21. J. G. Donaldson, C. L. Jackson, ARF family G proteins and their regulators: roles in membrane transport, development and disease. *Nature reviews Molecular cell biology* **12**, 362-375 (2011).
22. R. Beck *et al.*, Membrane curvature induced by Arf1-GTP is essential for vesicle formation. *Proceedings of the National Academy of Sciences* **105**, 11731-11736 (2008).
23. G. Tanigawa *et al.*, Hydrolysis of bound GTP by ARF protein triggers uncoating of Golgi-derived COP-coated vesicles. *The Journal of cell biology* **123**, 1365-1371 (1993).
24. M. J. Kraeutler, A. R. Soltis, J. J. Saucerman, Modeling cardiac β-adrenergic signaling with normalized-Hill differential equations: comparison with a biochemical model. *BMC systems biology* **4**, 1-12 (2010).
25. P. M. Tan, K. S. Buchholz, J. H. Omens, A. D. McCulloch, J. J. Saucerman, Predictive model identifies key network regulators of cardiomyocyte mechano-signaling. *PLoS Computational Biology* **13**, e1005854 (2017).
26. Y. D. Shaul, R. Seger, ERK1c regulates Golgi fragmentation during mitosis. *The Journal of cell biology* **172**, 885-897 (2006).
27. P.-L. Boulay, M. Cotton, P. Melançon, A. Claing, ADP-ribosylation factor 1 controls the activation of the phosphatidylinositol 3-kinase pathway to regulate epidermal growth factor-dependent growth and migration of breast cancer cells. *Journal of Biological Chemistry* **283**, 36425-36434 (2008).

28. E. Haines, S. Schlienger, A. Claing, The small GTPase ADP-Ribosylation Factor 1 mediates the sensitivity of triple negative breast cancer cells to EGFR tyrosine kinase inhibitors. *Cancer biology & therapy* **16**, 1535-1547 (2015).
29. E. Haines, C. Saucier, A. Claing, The adaptor proteins p66Shc and Grb2 regulate the activation of the GTPases ARF1 and ARF6 in invasive breast cancer cells. *Journal of Biological Chemistry* **289**, 5687-5703 (2014).
30. L. A. Cohen, J. G. Donaldson, Analysis of Arf GTP‐binding protein function in cells. *Current protocols in cell biology* **48**, 14.12. 11-14.12. 17 (2010).
31. B. M. Collins, P. J. Watson, D. J. Owen, The structure of the GGA1-GAT domain reveals the molecular basis for ARF binding and membrane association of GGAs. *Developmental cell* **4**, 321-332 (2003).
32. Y. Shiba *et al.*, GAT (GGA and Tom1) domain responsible for ubiquitin binding and ubiquitination. *Journal of Biological Chemistry* **279**, 7105-7111 (2004).
33. T. Shiba *et al.*, Molecular mechanism of membrane recruitment of GGA by ARF in lysosomal protein transport. *Nature structural biology* **10**, 386-393 (2003).
34. B. M. Collins, P. J. Watson, D. J. Owen, The structure of the GGA1-GAT domain reveals the molecular basis for ARF binding and membrane association of GGAs. *Developmental cell* **4**, 321-332 (2003).
35. N. A. Kalogriopoulos *et al.*, Structural basis for GPCR-independent activation of heterotrimeric Gi proteins. *Proceedings of the National Academy of Sciences* **116**, 16394-16403 (2019).
36. S. K. Gibson, A. G. Gilman, Giα and Gβ subunits both define selectivity of G protein activation by α2-adrenergic receptors. *Proceedings of the National Academy of Sciences* **103**, 212-217 (2006).
37. R. Brent, Cell signaling: what is the signal and what information does it carry? *FEBS letters* **583**, 4019-4024 (2009).
38. J. R. Lane *et al.*, Antibodies that identify only the active conformation of G(i) family G protein alpha subunits. *FASEB J* **22**, 1924-1932 (2008).
39. K. J. Åström, R. M. Murray, *Feedback systems: an introduction for scientists and engineers*. (Princeton university press, 2021).
40. C. R. Kime, M. M. Mano, *Logic and computer design fundamentals*. (Prentice Hall, 2003).
41. C. J. Gallione, J. K. Rose, A single amino acid substitution in a hydrophobic domain causes temperature-sensitive cell-surface transport of a mutant viral glycoprotein. *Journal of virology* **54**, 374-382 (1985).
42. A. Rahman-Zaman, S. Shan, C. A. Reinhart-King, Cell migration in microfabricated 3D collagen microtracks is mediated through the prometastatic protein girdin. *Cellular and molecular bioengineering* **11**, 1-10 (2018).
43. I. Lopez-Sanchez *et al.*, GIV/Girdin is a central hub for profibrogenic signalling networks during liver fibrosis. *Nature communications* **5**, 1-18 (2014).
44. R. J. Reddy *et al.*, Early signaling dynamics of the epidermal growth factor receptor. *Proceedings of the National Academy of Sciences* **113**, 3114-3119 (2016).
45. H. Cai, K. Reinisch, S. Ferro-Novick, Coats, tethers, Rabs, and SNAREs work together to mediate the intracellular destination of a transport vesicle. *Developmental cell* **12**, 671-682 (2007).
46. S. Uda *et al.*, Robustness and compensation of information transmission of signaling pathways. *Science* **341**, 558-561 (2013).
47. A. Kiyatkin, I. K. v. A. van Rosenburgh, D. E. Klein, M. A. Lemmon, Kinetics of receptor tyrosine kinase activation define ERK signaling dynamics. *Science Signaling* **13**, (2020).
48. R. D. Fritz *et al.*, A versatile toolkit to produce sensitive FRET biosensors to visualize signaling in time and space. *Science signaling* **6**, rs12-rs12 (2013).
49. K. K. Midde *et al.*, Multimodular biosensors reveal a novel platform for activation of G proteins by growth factor receptors. *Proceedings of the National Academy of Sciences* **112**, E937-E946 (2015).
50. S. Haney, L. Bardwell, Q. Nie, Ultrasensitive responses and specificity in cell signaling. *BMC systems biology* **4**, 1-14 (2010).
51. S. S. Andrews, W. J. Peria, C. Y. Richard, A. Colman-Lerner, R. Brent, Push-pull and feedback mechanisms can align signaling system outputs with inputs. *Cell systems* **3**, 444-455. e442 (2016).
52. S. S. Andrews, R. Brent, G. Balázsi, Signaling Systems: Transferring information without distortion. *Elife* **7**, e41894 (2018).
53. L. M. Stolerman, P. Ghosh, P. Rangamani, Stability analysis of a signaling circuit with dual species of GTPase switches. *arXiv preprint arXiv:2009.08356*, (2020).

54. K. Thurley, L. F. Wu, S. J. Altschuler, Modeling cell-to-cell communication networks using response-time distributions. *Cell systems* **6**, 355-367. e355 (2018).
55. A. P. Thomas, G. S. J. Bird, G. Hajnóczky, L. D. Robb‐Gaspers, J. W. Putney Jr, Spatial and temporal aspects of cellular calcium signaling. *The FASEB Journal* **10**, 1505-1517 (1996).
56. C. J. Gallione, J. K. Rose, A single amino acid substitution in a hydrophobic domain causes temperature-sensitive cell-surface transport of a mutant viral glycoprotein. *Journal of virology* **54**, 374-382 (1985).

FIGURES AND LEGENDS

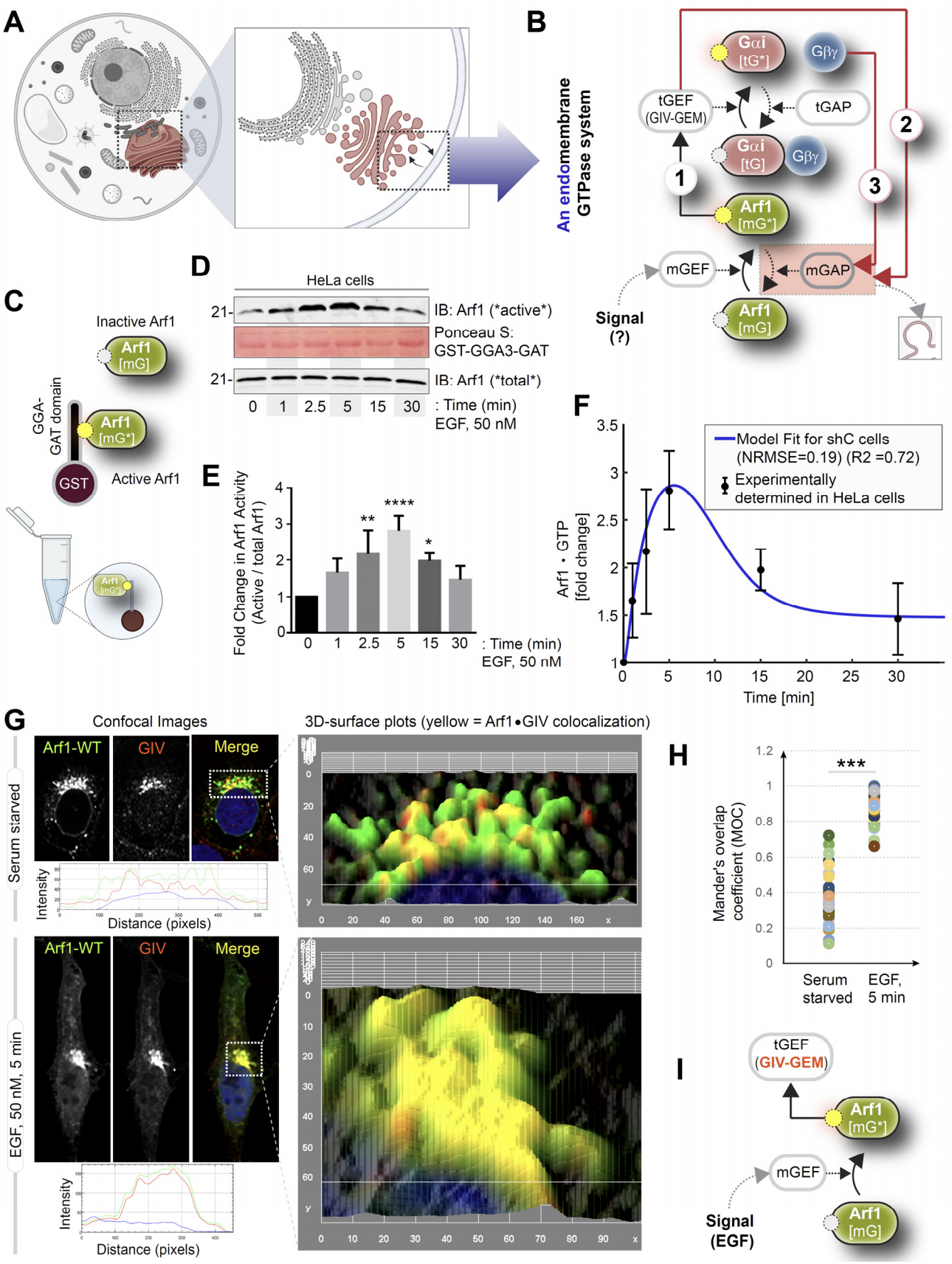

FIGURE 1

Figure 1. EGF activates Arf1 (mG*) within the Golgi-localized endomembrane GTPase system, triggers the recruitment of GIV-GEM on Golgi.

A. Schematic shows a Golgi-localized endomembrane GTPase system comprised of two distinct species of GTPases, monomeric (m) and trimeric (t), which regulates Golgi processes.

B. Components of that system are shown on left. Arrows denote key molecular events/chemical reaction cascades within this system, in which, the GIV-GEM links monomeric (m) and trimeric (t) GTPase systems and enable the conversion of extracellular stimuli (ligand; left) into membrane trafficking events (e.g., vesicle uncoating/budding/fusion; right). See also **Figure S1** for illustrations detailing the sequential steps within the dynamic nature of the motif.

C. Schematic outlines the biochemical approach to studying the proportion of Arf activation in cells using GST-GGA-GAT domain. Bound fraction represents active and unbound fraction represents inactive conformation.

D. Immunoblot shows bound Arf1 (active; top) and total Arf1 (input lysates; bottom) from equal aliquots of lysates of HeLa cells that were stimulated with EGF for the indicated time points prior to lysis.

E. Bar graphs display the fold change in Arf1 activity normalized to t0 min. Results are expressed as mean ± S.E.M; n = 3 replicates; *p* values were determined using Mann-Whitney t-test compared to t0: *, <0.05; **, <0.01; ***, <0.001. Immunoblots are representative of findings from at least 3 independent repeats.

F. Graph displays an overlay of experimentally determined Arf1 activation dynamics (results are displayed as mean ± S.D) and model-derived simulation (blue continuous line) in control cells where m and t-GTPases are coupled.

G. HeLa cells expressing Arf1-HA were serum starved overnight (G, top) and subsequently stimulated with EGF for 5 min (G, bottom) prior to fixation with PFA. Fixed cells were stained for Arf1 (HA; green) and GIV (red) and nuclei (DAPI; blue). Panels on the left show overlay of all 3 stains and representative RGB plots of sections through the Arf1-stained pixels. Panels on the right display the magnified 3D surface plots of the boxed regions in the left panels.

H. Scatter plot shows the Mander's overlap coefficient (MOC) for Arf1-HA and GIV colocalization in G that was calculated on 13-15 cells/experiment, n = 3 independent experiments. *p* values were determined using Mann-Whitney t-test: ***, <0.001.

I. Schematic summarizing the experimentally determined steps within the Golgi-localized endomembrane GTPase system that are triggered by EGF.

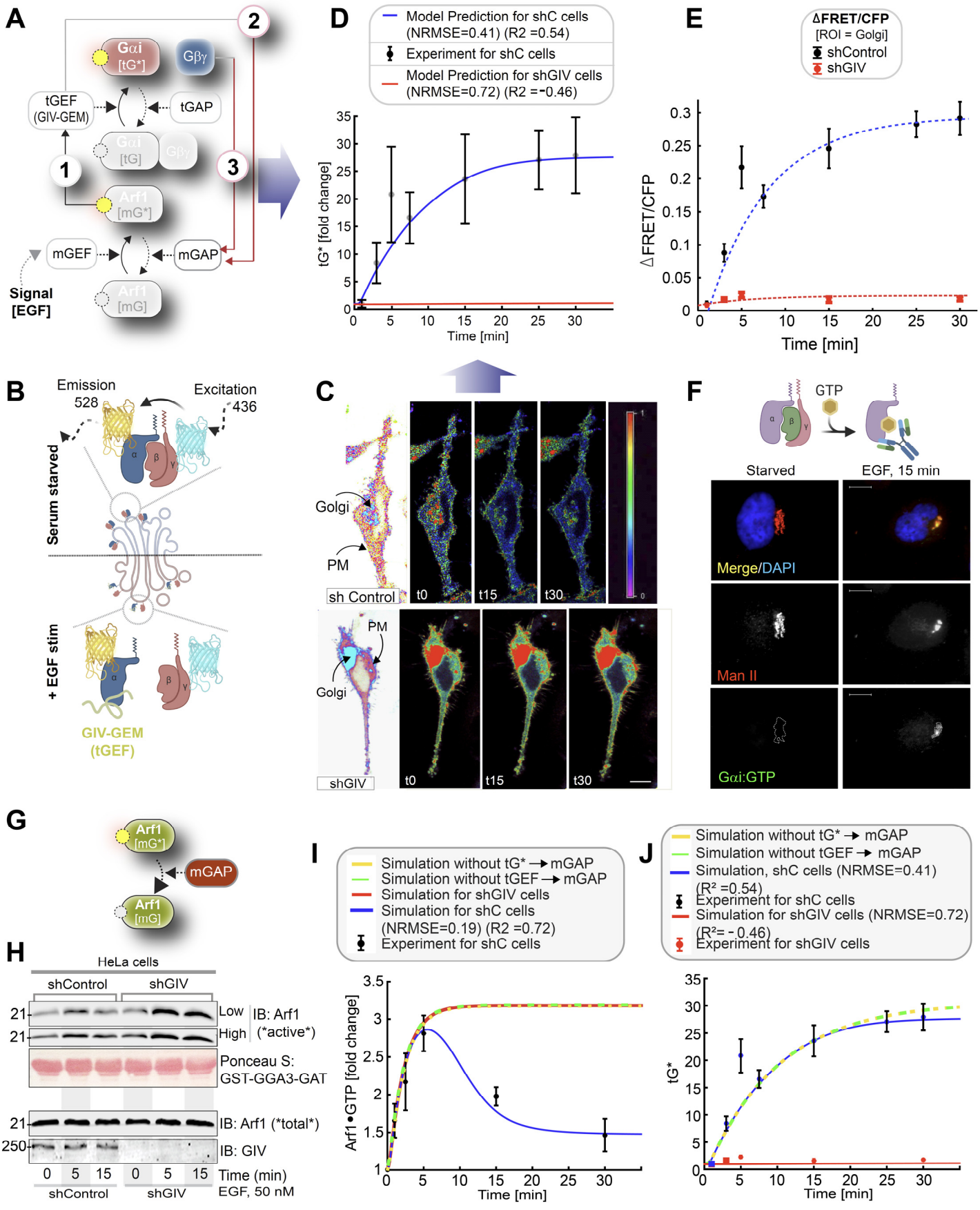

FIGURE 2

Figure 2. EGF triggers activation of Gi (tG*) on Golgi membranes and terminates Arf1 signaling, requires GIV-GEM.

A. Schematic shows the specific step within the endomembrane GTPase system being interrogated in this figure.

B. Schematic describing the mechanism of the FRET Gαi activity reporter. Serum starved conditions are expected to have more inactive trimeric Gi, and hence show high FRET (top). Upon ligand stimulation GIV-dependent dissociation of trimers is expected, with a resultant loss of intermolecular FRET.

C. Control (sh Control; top) and GIV-GEM depleted (shGIV; bottom) HeLa cells were co-transfected with Gαi1-YFP, Gβ1-CFP and Gγ2 (untagged) and live cells were analyzed by FRET imaging at steady-state, after being serum starved in 0.2% FBS overnight and then after stimulation with 50 nM EGF. Representative freeze-frame FRET images are shown. FRET image panels display intensities of acceptor emission due to efficient energy transfer in each pixel. FRET scale is shown in inset. Golgi and PM regions of interest are indicated with arrows. Scale bar = 10 μm. See also **Figure S2A** for free-frame images for additional time points in control HeLa cells.

D-E. Continuous line graphs in D displays the model-derived simulation of the EGF-triggered kinetics of tG* activation at the Golgi in shControl (blue) and shGIV cels (red). Overlayed experimentally derived data (derived from E) is represented as error bars (± S.D). Interrupted line graphs in E display the quantification of FRET results from during a 30 min period after EGF stimulation. Results are expressed as mean ± S.E.M. Data represent 5 regions of interest (ROIs) analyzed over the pixels corresponding to the Golgi of 3-5 cells from 5 independent experiments. *p* values, as determined against t0 using Mann-Whitney were ****, <0.0001 for all time points t5-t30 min. Continuous line graph in D displays the model-derived simulation of the EGF-triggered kinetics of tG* activation at the Golgi, overlayed on experimentally derived data, represented as error bars.

F. *Top*: Schematic showing how a conformation-specific anti-Gαi•GTP antibody detects GTP-bound active Gαi in situ. *Bottom*: HeLa cells starved with 0.2% FBS overnight or stimulated subsequently with 50 nM EGF were fixed and stained for active Gαi (green; anti-Gαi:GTP mAb) and Man II (red) and analyzed by confocal microscopy. Activation of Gαi was detected exclusively after EGF stimulation. When detected, active Gαi colocalizes with Man II (yellow pixels in merge panel). See also **Figure S2B** for additional time points and stimuli. Scale bar = 7.5 μm.

G. Schematic shows the step within the endomembrane GTPase system being interrogated in panels H-J.

H. Immunoblot in C shows bound Arf1 (active; top) and total Arf1 (input lysates; bottom) from equal aliquots of lysates of control (sh Control) and GIV-depleted (shGIV) HeLa cells that were stimulated with EGF for the indicated time points prior to lysis. Bar graphs in **Figure S3A** display the fold change in Arf1 activity normalized to t0 min.

I. Line graphs display the model-derived simulations of Arf1 activation dynamics (mG*) in cells without tGEF (shGIV; red), or for other conditions in which one or the other negative feedback loops are missing (interrupted yellow and green continuous line graphs). As a reference, results of model-derived simulation fit to experimental data in control cells are displayed in blue.

J. Line graphs display the model-derived simulations of Gαi (tG*) activation dynamics in cells without tGEF (shGIV; red), or for other conditions in which one or the other negative feedback loops are missing (interrupted yellow and green continuous line graphs). As a reference, results of model-derived simulation fit to experimental data in control cells are displayed in blue.

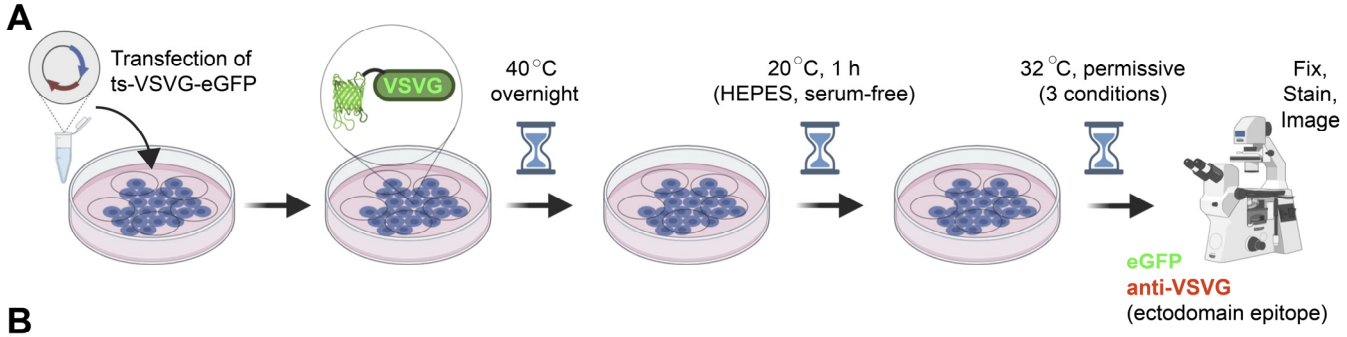

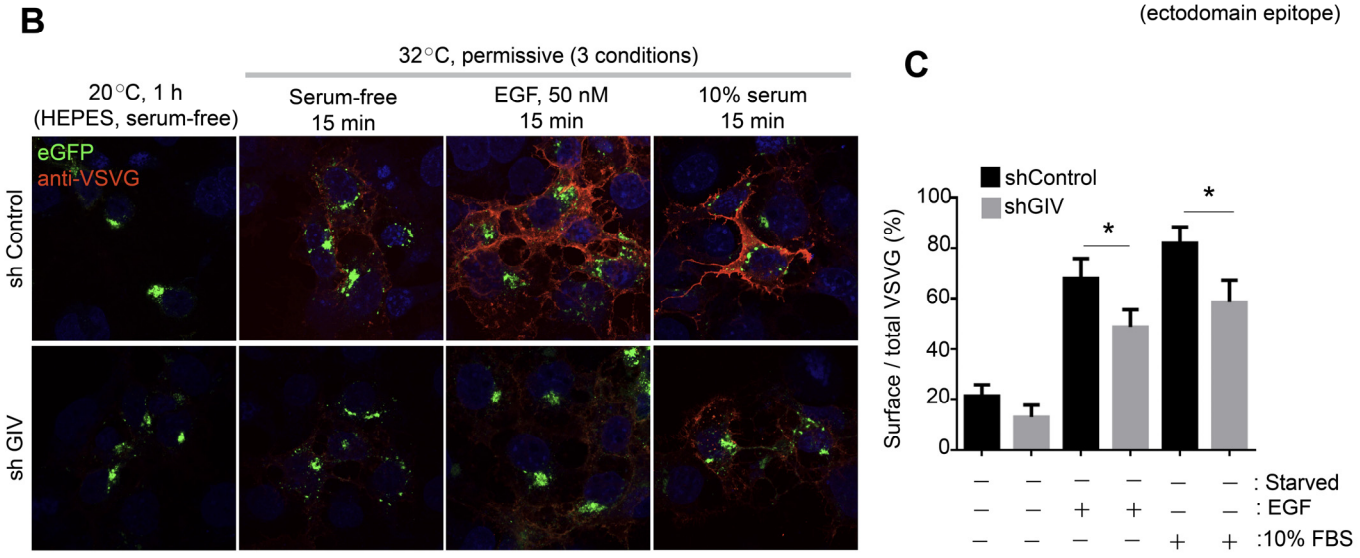

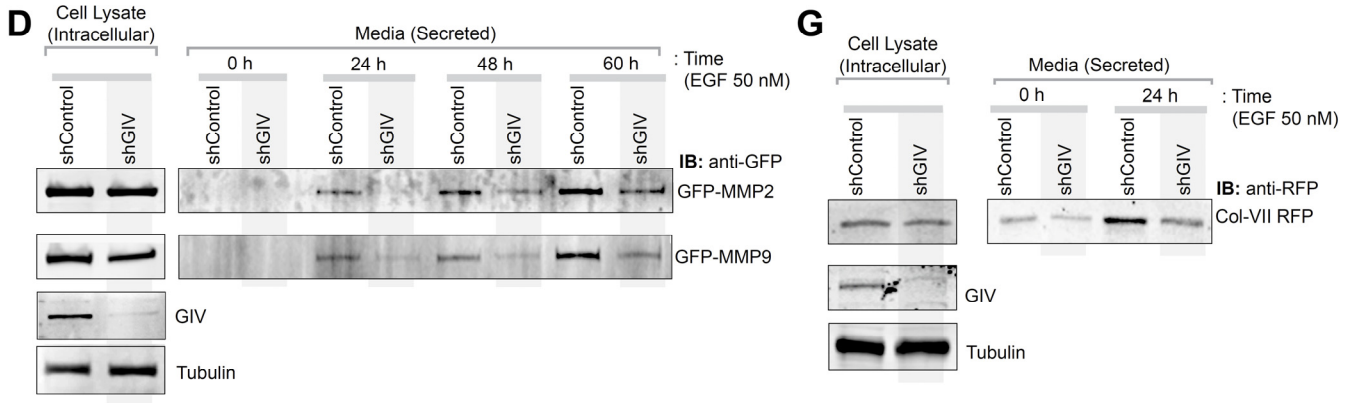

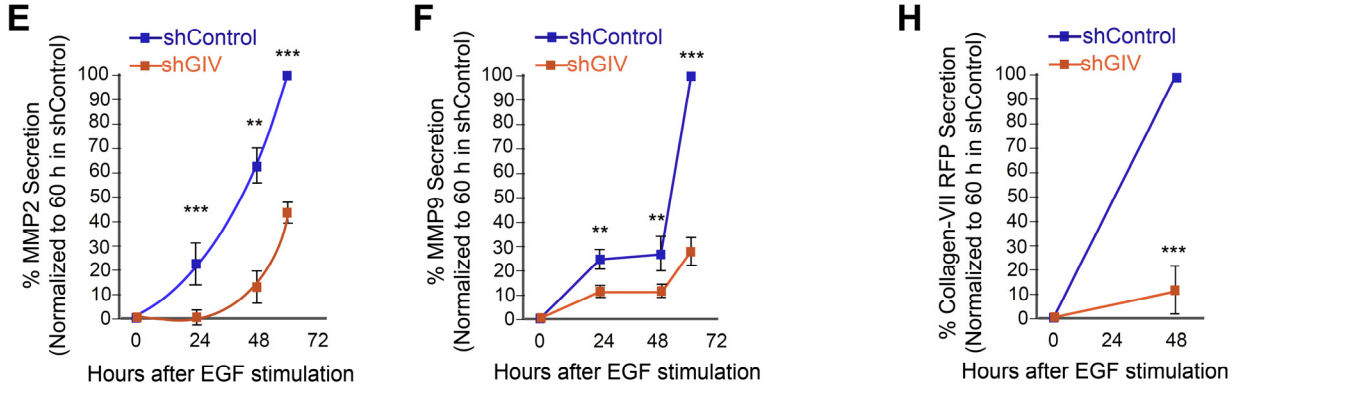

FIGURE 3

Figure 3. **GIV-GEM is required for EGF-triggered secretion of diverse cargo proteins through Golgi compartment.**

A. Schematic shows the basis for measuring secretion of transmembrane cargo protein, ts-VSVG-eGFP. This temperature-sensitive mutant VSVG is retained in the ER at 40°C, at the Golgi at 20°C, and moves out of the Golgi to the PM when shifted to 32°C (*56*). When visualized with immunofluorescence under non-permeabilized conditions, a VSVG-ectodomain targeting antibody selectively detects PM-localized cargo, whereas GFP tag allows the visualization of total VSVG in the cell.

B-C. Control (sh Control; top) and GIV-depleted (shGIV; bottom) Cos7 cells were transfected with tsO45-VSVG-GFP and cells were shifted to 40°C for O/N and then incubated at 20°C for 1 h in HEPES buffered serum free media followed by temperature shift at 32°C for 15 minutes in plain DMEM and or containing 50nM EGF or 10% serum. Coverslips were fixed and stained with VSVG-ectodomain specific monoclonal antibody (red). Representative images are shown in B. Green fluorescence indicates total VSVG expression whereas red fluorescence shows surface-localized pool of VSVG. Bar graphs in C display the Red:Green intensity ratio indicative of fraction VSVG that is secreted to the cell surface. Results are expressed as mean ± S.E.M; n = 3 replicates; *p* values were determined using Mann-Whitney t-test compared to t0: *, <0.05.

D-H. Control (sh Control) and GIV-depleted (shGIV) HeLa cells were analyzed for EGF-stimulated secretion of three soluble cargo proteins, MMP2 (D, E), MMP9 (D, F) and Collagen-Vii RFP (G, H), as detected from the supernatants at indicated time points after EGF stimulation. Results are expressed as mean ± S.E.M; n = 3 replicates; *p* values were determined using Mann-Whitney t-test compared to t0: *, <0.05; **, <0.01; ***, <0.001. Immunoblots are representative of findings from at least 3 independent repeats.

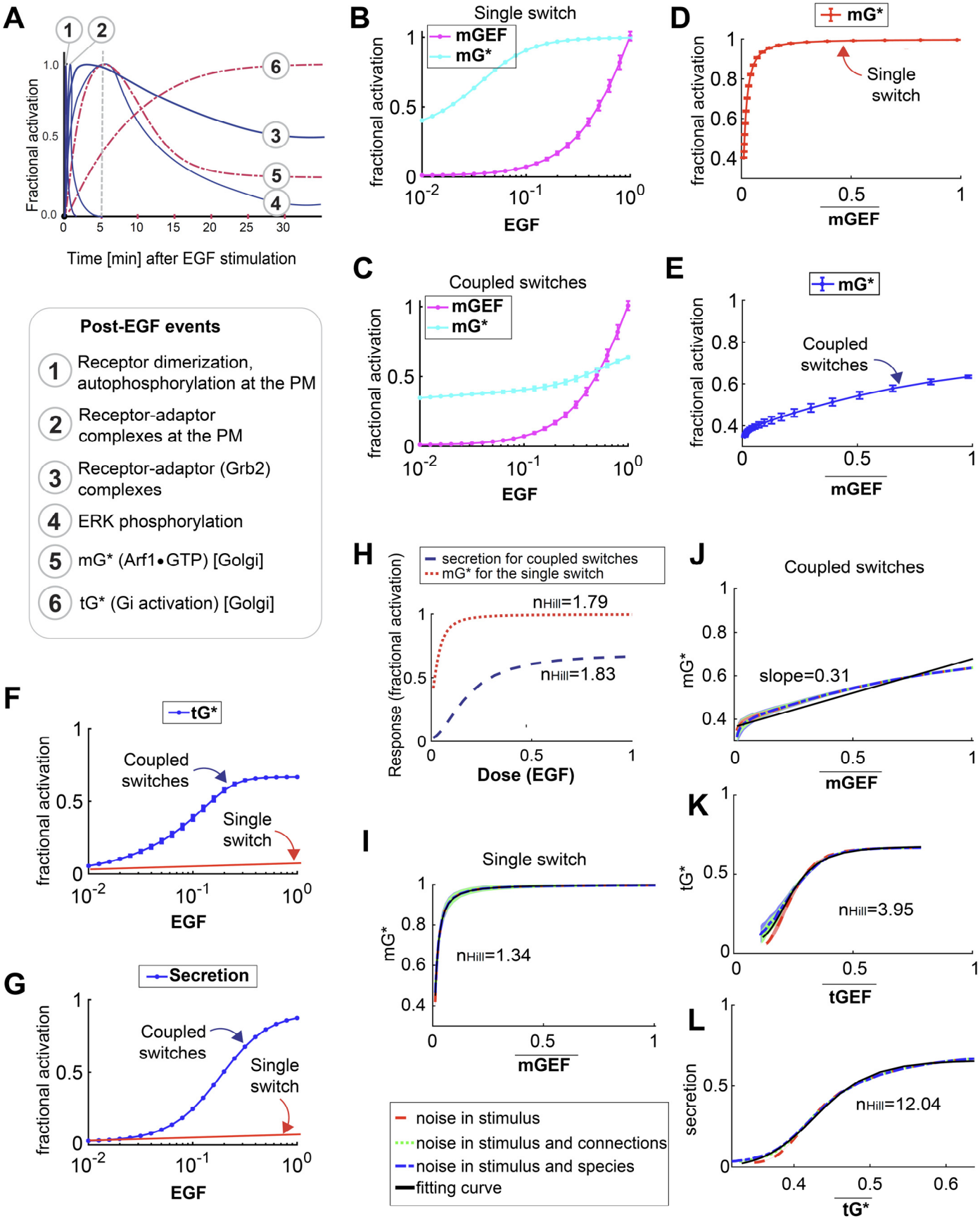

FIGURE 4

Figure 4. Coupled switches enable the alignment of endomembrane responses (Arf1 activity and Golgi secretory functions) to the dose of extracellular stimuli.

A. Published dynamics of EGF-stimulated events that are initiated at the PM (blue, continuous) or experimentally determined dynamics of events at the Golgi confirmed here (red, interrupted) are compared.

B-C. Dose responses of fractional activations of mGEF and mGTPase for the single switch (B) and coupled switches (t). We perform stochastic simulations in the presence of noise in EGF (see Supplemental Material for details). The mean and the standard deviation (SD) of species are evaluated at [illegible]=24 h. Data are shown as mean ± SD for 1000 repeated simulations. In all simulations, the initial condition represents the starved state when *stimulus*=0, and then *stimulus* is set to be 0.23 to simulate the experimental conditions, i.e., 50 nM EGF. The dimensionless EGF concentrations in the simulations are obtained through normalization, i.e., dividing the EGF concentration by 217.4 nM (=50 nM/0.23).

D-E. Relationships between active Arf1 and mGEF for the single switch (D) and coupled switches (E). Data are shown as mean values, which are the same as those in (B-C).

F-G. Dose responses of fractional activations of tGTPase (F) and secretion (G) for coupled switches and the single switch. Data for coupled switches are obtained in the same way as in (C) and are shown as mean ± SD. For the single switch, schematic plots are used.

H. Dose responses of secretion for coupled switches and mGTPase for the single switch. The Hill function $\frac{kx^n}{K+x^n} + d$ is used to fit the dose-response curve, and the best-fit value of the Hill coefficient n_{Hill} is shown (r^2>0.98 for both curves).

I-J. Relationships between active Arf1 and mGEF for the single switch (I) and coupled switches (J). The mean and SD of species at t=24 h are calculated in the presence of three different types of noise: noise in stimulus (shown in red), noise in stimulus and connections simultaneously (shown in green), and noise in stimulus and species simultaneously (shown in blue) (see also Supplemental Material for details). $\overline{mGEF}$ denotes the mean of mGEF. The dashed line shows the mean of the fractional activation of mGTPase, with the shading indicating the SD. The fitting curves and n_{Hill}'s (r^2>0.98) are calculated in the same way as in (H).

K-L. The tGTPase activation versus tGEF (K), and the secretion versus active tGTPase (L) for coupled switches. These two plots are generated in a similar way as described in (J). r^2>0.98 for both fitting curves.

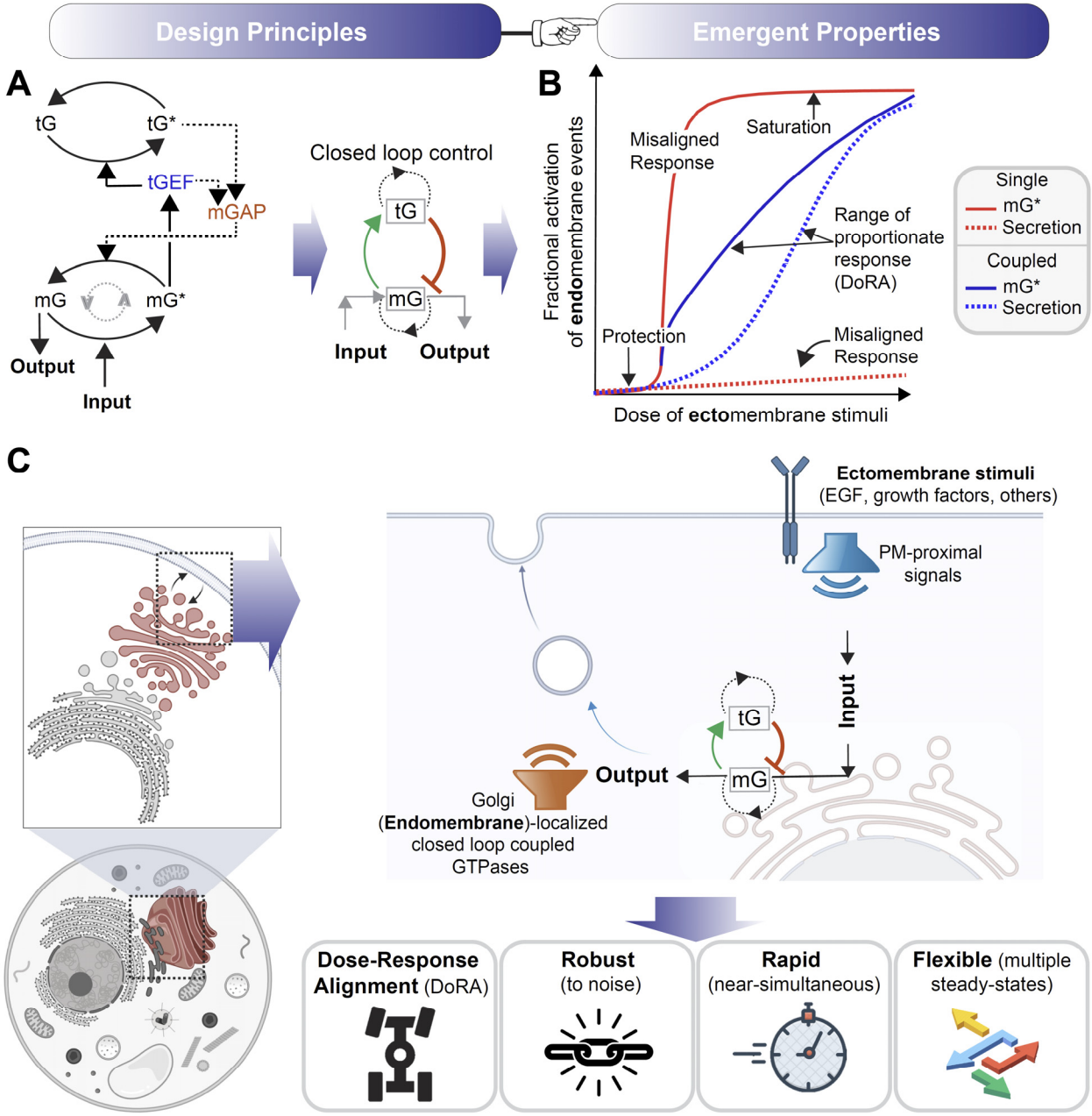

FIGURE 5

Figure 5. **Summary of findings: the design principles (A) and emergent properties (B) of the closed loop control for coupled switches.**

A. Schematic illustrating. mG denotes the first of two switches, the mGTPase Arf1, and tG denotes the second of the two switches, the tGTPase Giαβγ.

B. Schematic diagram of dose responses (mG* and secretion) for the single switch and coupled switches. Coupled switches stretch the range of proportionate responses. Single mG switch results in misaligned responses. DoRA, dose response alignment.

C. Schematic showing the impact of the closed loop control system on endomembrane responses, making the latter aligned to doses of growth factor stimuli, robust to noise, rapid and yet, flexible. These are likely responsible for rendering concordant Golgi responses.